Contribution from the Department of Chemistry,
Iowa State University, Ames, Iowa 50011

Heterometallic Condensed Cluster Compounds: Pr_4I_5Z (Z = Co, Ru, Os) and La_4I_5Ru. Synthesis, Structure, and Bonding

Martin W. Payne, Peter K. Dorhout, and John D. Corbett*

Received September 4, 1990

The title R_4I_5Z compounds are synthesized in high yield by reaction of R and RI_3 with Ru, Os, or CoI_2 at 875–975 °C in welded Nb containers. The yields of these Ru and Os compounds vs other phases appear to be significant functions of temperature. The structure of Pr_4I_5Ru was refined from single-crystal data as isotypic with Y_4I_5C ($C2/m$, $Z = 2$, $a = 19.110$ (5) Å, $b = 4.2654$ (9) Å, $c = 9.194$ (3) Å, $\beta = 104.55$ (2)°; R, $R_w = 4.1$, 6.4%). The phase consists of Ru-centered, Pr_6I_{12}-type clusters that share trans metal edges and iodine to generate quasi-infinite chains. The nominal Pr_6 octahedra therein are more uniformly proportioned than previously observed in chain structures, but the apical Pr–Ru bond is shorter than the waist Pr–Ru bond by 0.327 (1) Å. The magnetic susceptibility of Pr_4I_5Ru is Curie–Weiss in character with 7.1 μ_B/formula unit while La_4I_5Ru behaves like a Pauli paramagnet, $\chi = \sim 5.0 \times 10^{-4}$ emu/(mol Oe) after correction for core diamagnetism. The bonding in Pr_4I_5Ru has been considered in terms of the results of charge-consistent, extended-Hückel band calculations. Pr–I and Ru–Pr bonding is dominant, the Ru–Pr bonding states lying at the bottom of a Pr–Pr- and Pr–Ru-based conduction band crossed by E_F. Charges calculated for the two metals are similar and slightly positive, indicating the importance of covalence. The marked compression of the apical Pr–Ru bonds relative to distances in chain analogues centered by the main-group elements C or Si results from unequal π bonding within the distorted octahedra by the d orbitals of Ru.

Introduction

The surprises that exploratory synthesis can provide now include a considerable variety of condensed cluster iodides of rare-earth metals in which each cluster is centered by a late transition metal. Originally, we were astonished to discover that isolated rare-earth-element clusters in any form could be centered by other metals. The first metal interstitials (Z) were the 3d elements Mn–Ni in $R^{3+}[R_6I_{12}Z^{3-}]$ phases, R = Sc, Y, Pr, Gd.[1] This was followed by the encapsulation of not only each of the platinum metals but also of Re, Cu, or Au within $R_7I_{12}Z$ and related $R_6I_{10}Z$ examples for most of the same R.[2,3] There is no precedent, however, for metal-centered clusters condensed into nominally infinite chains, although rare-earth-metal examples centered by light non-metals, primarily carbon, are known, e.g., $Sc_7Cl_{10}C_2$,[4] Y_4I_5C and $Y_6I_7C_2$,[5] $Gd_{12}I_{17}C_6$, and others.[6] In addition, condensed cluster networks have also been found in Gd_4I_5Si and Gd_3I_3Si[7] as well as double-metal sheets in $Gd_2Cl_2C_2$, $Gd_6Cl_5C_3$, and so forth.[8]

The present article reports on R_4I_5Z compounds, the first of a sizable family of extended cluster iodides that are centered by heavy transition metals and occur in both known and new structure types. The explorations again feature mainly the hosts R = Y, Pr, Gd, although we have also included lanthanum in the study in order to gain a phase with diamagnetic cores after yttrium was found to yield this composition only in a different structure.

Experimental Section

Syntheses. The high purity of the rare-earth metals employed, the synthetic and vacuum sublimation techniques for the corresponding RI_3 phases, the origin and purities of the interstitial sources employed, and the Guinier powder pattern methods have all been described before.[1-3] The syntheses of R_4I_5Z phases generally utilized stoichiometric proportions of powdered Y, Pr, Gd, or La turnings together with the corresponding RI_3 and powdered elemental Z (or CoI_2) in welded Nb tubing. About 5% ROI is a rather common contaminant at the temperatures employed.

Table I. Lattice Dimensions (Å, deg) of Pr_4I_5Ru and Other Analogues[a]

	a	*b*	*c*	β
La_4I_4Ru	19.500 (6)	4.3136 (9)	9.403 (3)	104.85 (3)
Pr_4I_5Co	19.013 (2)	4.2616 (4)	9.1998 (8)	104.35 (1)
Pr_4I_5Ru	19.110 (5)	4.2654 (9)	9.194 (3)	104.55 (2)
Pr_4I_5Os	19.200 (3)	4.2570 (9)	9.292 (3)	104.59 (2)
Y_4I_5C[b]	18.479 (6)	3.947 (1)	8.472 (3)	103.22 (4)
Gd_4I_5Si[c]	18.917 (2)	4.1966 (4)	8.7099 (9)	103.30 (1)

[a] Space group $C2/m$. [b] From ref 5. [c] From ref 7.

The diverse stability ranges of the new products and the presence of alternate phases in competition became evident as the synthetic conditions were explored. Needles of Pr_4I_5Ru from which the structure and composition were established were first encountered following an attempted synthesis of (unknown) $Pr_6I_{10}Ru$ that was run at a somewhat higher than normal temperature, 950 °C, for 22 days. The known $Pr_7I_{12}Ru$ was the major product. Later reactions employing the correct stoichiometry gave, surprisingly, appropriate proportions of $Pr_7I_{12}Ru$ and $Pr_6I_6Ru_2$[9] at 900 °C but afforded the phase of interest in ~95% yield at 950–975 °C (26–30 days). $Pr_6I_6Ru_2$ is also formed in systems with a lower iodine content. It also proved possible to synthesize the isostructural Pr_4I_5Co and Pr_4I_5Os. The cobalt example is also a product of reactions at 900–950 °C with lower iodine contents, in contrast to many instances where R_3I_3Z compositions intrude. As with Pr_4I_5Ru, the formation of Pr_4I_5Os requires a higher temperature, at least 875–900 °C for 28 days; $Pr_7I_{12}Os$ and $Pr_6I_{10}Os$ are obtained at 800 °C. The reverse, disproportionation reactions that are implied at lower temperatures were not investigated.

Negative results (i.e., other phases, some new and interesting in their own right) were encountered from attempts to incorporate Z = Re, Ir, Rh, Pt, Fe, Cu, Ag in Pr_4I_5Z. As before,[3] no cluster phases of any kind formed with Z = V, Cr, Mo, Ag.

Strangely enough, neither Gd_4I_5Z nor Y_4I_5Z structural analogues could be obtained. The often versatile yttrium gave $Y_6I_{10}Z$ for Z = Os, Co, Rh, Ir, Pt as well as $Y_7I_{12}Fe$, Y_3I_3Ir, and Y_4I_5Ru in a new structure type.[10] Lanthanum reactions at 975 °C provided a high yield of La_4I_5Ru in the form of needles up to 2 mm in length, but mixtures were produced at 850 °C. The structure of interest was not obtained for Z = Re, Os, Ir, Rh. The Guinier-based lattice dimensions of most of the new R_4I_5Z phases as well as related examples are given in Table I. The data given for Pr_4I_5Ru are diffractometer results; its Guinier pattern contains an unusual proportion of weak and somewhat broad lines, and the lattice parameters refined therefrom were consistent but of lower precision.

Crystallography. Single needle crystals of what turned out to be Pr_4I_5Ru were sealed in thin-walled capillaries and studied on a Rigaku

(1) Hughbanks, T.; Corbett, J. D. *Inorg. Chem.* **1988**, *27*, 2022.
(2) Hughbanks, T.; Corbett, J. D. *Inorg. Chem.* **1989**, *28*, 631.
(3) Payne, M. W.; Corbett, J. D. *Inorg. Chem.* **1990**, *29*, 2246.
(4) Hwu, S.-J.; Corbett, J. D.; Poeppelmeier, K. R. *J. Solid State Chem.* **1985**, *57*, 43.
(5) Kauzlarich, S. M.; Hughbanks, T.; Corbett, J. D.; Klavins, P.; Shelton, R. N. *Inorg. Chem.* **1988**, *27*, 1791.
(6) Simon, A. *Angew. Chem., Int. Ed. Engl.* **1988**, *27*, 177.
(7) Nagaki, D.; Simon, A.; Borrmann, H. *J. Less-Common Met.* **1989**, *156*, 193.
(8) Simon, A.; Schwarz, C.; Bauhofer, W. *J. Less-Common Met.* **1988**, *137*, 343.
(9) Payne, M. W.; Corbett, J. D. To be published.
(10) Payne, M. W.; Ebihara, M.; Corbett, J. D. *Angew. Chem.*, submitted for publication.

0020-1669/91/1330-1467$02.50/0

Table II. Some Crystal and Refinement Data for Pr_4I_5Ru[a]

space group, Z	$C2/m$ (No.12), 2
V, Å^3	725.4 (6)
μ(Mo Kα), cm^{-1}	248.3
transm coeff range	0.660–1.000
no. of data with $F_o^2 > 3\sigma(F_o^2)$	849
no. of params refined	33
R,[b] %	4.1
R_w,[c] %	6.4

[a] Lattice dimensions are listed in Table I. [b] $R = \sum||F_o| - |F_c||/\sum|F_o|$. [c] $R_w = [\sum w(|F_o| - |F_c|)^2/\sum w(F_o)^2]^{1/2}$; $w = (\sigma(F))^{-2}$.

AFC6R diffractometer at room temperature. Preliminary orientation tuning indicated a probable C-centered monoclinic cell with proportions appropriate to many cluster chain phases. However, data were collected and the structure was solved for a different primitive monoclinic lattice in order to check this. No decay in standard reflections with time was found. Adsorption was corrected with the aid of two ψ scans. Direct methods (MITHRIL) readily gave all atoms in the structure, and their refinement was uneventful. The reflection indices and the atom positions were then converted to the $C2/m$ cell and further refined when it became clear that the results were within experimental errors of those for this cell. (The converted reflection data also supported the C-centering condition.) The occupancy of Ru refined to 100.1 (6)% and was thereafter fixed at unity. The largest residuals in the final difference Fourier map were peaks of 2.2 e/Å^3, 1.8 Å from Ru, and 2.1 e/Å^3, 1.0 Å from Pr2. Ripples in the Fourier map up to 9 e/Å^3 suggested a truncated data set had been obtained within the $2\theta = 55°$ limit. Dropping three reflections that had $\Delta F/\sigma(F) > 20$ reduced R_w from 6.4% to 5.0%. Some details of the data collection and refinement without this exclusion are given in Table II.

Magnetism. Magnetic susceptibility measurements on Pr_4I_5Ru and La_4I_5Ru were performed on a Quantum Design-MPMS SQUID magnetometer at 1000 G over a temperature range 6–300 K with measurements every 10 K. Quantitative samples (40–50 mg) were sealed in silica tubes under 100 Torr of He.

Calculations. In order to examine Pr–Pr and Pr–Ru bonding in Pr_4I_5Ru, one-dimensional extended Hückel band structure calculations[11] were carried out at 16k points for the chain $^1_\infty[Pr_4I_8Ru^{3-}]$ in which terminal iodine atoms had been added at all exo positions to simulate the bridge bonding. The X-ray refinement data yield a Brillouin zone that contains only a C_{2x} axis common to the chain axis (x). In order to facilitate band symmetry assignments, a similar treatment was also performed with slightly altered parameters so as to generate the two pseudomirror planes xy (waist Pr1, Ru) and xz (apex Pr2, Ru) along the chain axis, the intersection of which coincides with the original C_2 axis. The results for the two models differed insignificantly for our purposes, and therefore the idealized version has been adopted for bonding considerations. Some minor band crossings were introduced thereby that were avoided with the actual structure.

Tabulated input parameters were used for Pr[12,13] in the calculations and in modeling the variations of H_{ii} (valence state energy) with occupancy, while those for I and Ru were taken from an earlier self-consistent study on $Y_6I_{10}Ru$.[2] Self-consistent charges on Pr were achieved via iterative calculations on the present system, giving H_{ii} data for Pr as follows: 6s, −4.70 eV; 6p, −4.70 eV; 5d, −7.58 eV. The last datum compares with a starting value of −7.28 eV based on atomic Pr. Orbital parameters were not varied. A smoothing parameter of 0.005 eV was applied to the DOS and COOP plots.

Results and Discussion

Synthesis. We previously established that the cluster phases $R_6I_{10}Z$ and $R_7I_{12}Z$ are obtained in high yields in many of the systems studied here when the synthesis reactions are run with the appropriate stoichiometries, in accord with the phase rule.[1-3] However, the importance of varying the synthetic compositions and temperatures from presupposed values has become evident during later studies when a variety of extended chain and network structures involving many of the same elements were also discovered. Furthermore, stoichiometric reactions aimed at Pr_4I_5Ru, Pr_4I_5Os, or La_4I_5Ru that were run at 800–900 °C were found to produce other phases containing both discrete and extended clusters, whereas in each case a reaction carried out only 50–125 °C higher give a high yield of the target phase (see Experimental Section). It is difficult to believe that such sharp temperature dependencies for the formation of these R_4I_5Z phases during reaction periods of 3–4 weeks are kinetic in character; rather, these must represent changing equilibrium interrelationships between phases of very similar stabilities. The chances that the right synthetic conditions could be missed under such circumstances probably merit increased concern on the part of investigators. Of course, the appropriate conditions may also depend very much on just what other phases are stable. Thus, the existence of Pr_4I_5Co was considerably easier to establish because only the cluster compound $Pr_7I_{12}Co$, not other extended phases, appears

Table III. Positional and Isotropic Equivalent Thermal Parameters[a]

atom	x	z	B_{iso}, Å^2
Pr1	0.00157 (4)	0.2205 (1)	1.85 (3)
Pr2	0.35887 (4)	0.92625 (8)	1.53 (3)
I1	0.17235 (4)	0.3433 (1)	1.64 (4)
I2	0.17237 (4)	0.8291 (1)	1.57 (4)
I3	$^1/_2$	$^1/_2$	2.66 (6)
Ru	$^1/_2$	0	1.83 (6)

[a] $y = 0$.

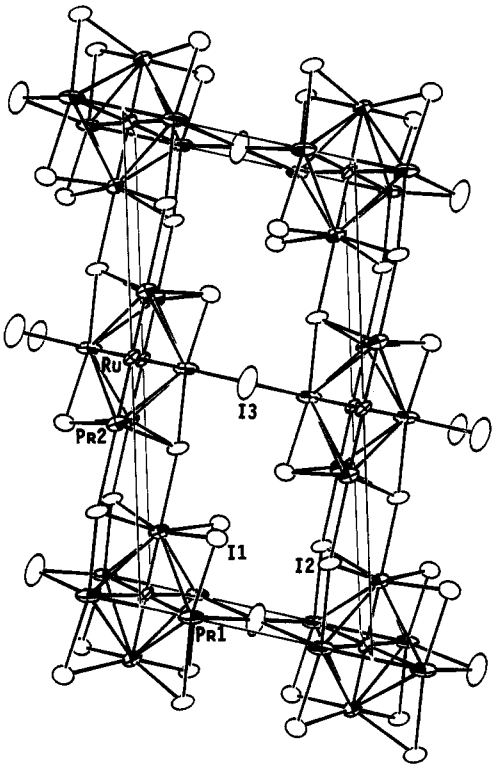

Figure 1. [010] view along the chains of the unit cell contents and interchain bonding in Pr_4I_5Ru. Pr atoms are shaded; Ru atoms are crossed; iodine atoms are open (90% probability) ellipsoids. The a axis lies vertical.

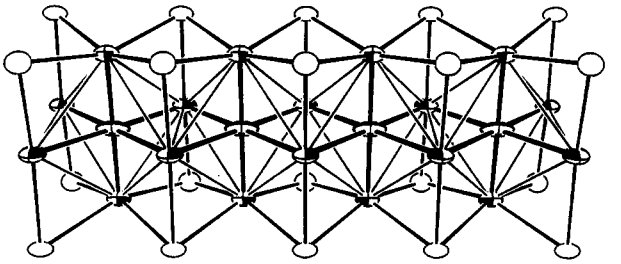

Figure 2. Portion of one nominally infinite chain in Pr_4I_5Ru with line widths approximating bond strengths. The I3 atoms that bridge between chains are not shown.

(11) (a) Hoffmann, R. *J. Chem. Phys.* **1963**, *39*, 1397. (b) Whangbo, M.-H.; Hoffmann, R. *J. Am. Chem. Soc.* **1978**, *100*, 6093. (c) Ammeter, J. H.; Bürgi, H.-B.; Thibeault, J. C.; Hoffmann, R. *J. Am. Chem. Soc.* **1978**, *100*, 3686.
(12) Ortiz, J. V.; Hoffmann, R. *Inorg. Chem.* **1985**, *24*, 2095.
(13) Clement, E.; Roetti, C. *At. Nucl. Data Tables* **1974**, *14*, 177.

Table IV. Important Distances (Å) and Angles (deg) in Pr_4I_5Ru

distances[a]		angles	
Pr1–Ru	2.9377 (8)	Pr1–Ru–Pr1	86.90 (3)
Pr2–Ru	2.611 (1)	Pr2–Ru–Pr2	180
Pr1–Pr1	4.041 (2)	Pr1–Ru–Pr2	89.43 (2)
Pr1–Pr2	3.910 (1)	I1–Pr1–I2	167.71 (4)
Pr1–Pr2	3.949 (1)	I1–Pr1–I3	86.21 (3)
Pr1–I1	3.174 (1)	I2–Pr1–I3	84.34 (3)
Pr1–I2	3.240 (1)	I3–Pr1–I3	79.22 (3)
Pr2–I1	3.210 (1)	I1–Pr2–I1	83.29 (3)
Pr2–I2	3.262 (1)	I1–Pr2–I2	79.67 (3)[b]
Pr2–I2	3.450 (2)[b]	I1–Pr2–I2	159.41 (3)
Pr1–I3	3.3452 (9)[b]	I1–Pr2–I2	93.85 (3)
I1–I1	4.167 (2)[b,c]	I2–Pr2–I2	79.76 (3)
		I2–Pr2–I2	81.67 (3)
		Pr1–I3–Pr1	79.22 (3)[b]

[a] All atoms also have two like neighbors along the chain at 4.2654 (9) Å (*b*). [b] Interchain interaction. [c] All d(I–I) < *b*.

Table V. Comparative Distances (Å) in R_4I_5Z Phases

	distance	Pr_4I_5Ru	Gd_4I_5Si[a]	Y_4I_5C[b]
1	R1–R1 axial repeat (*b*)	4.265	4.197	3.947
2	R1–R1 shared edge	4.041	3.733	3.248
3	R1–R2 (wasit–apex, av)	3.930	3.914	3.512
	Δ(2–3)	0.111	−0.181	−0.264
4	R1–Z (waist) (×2)	2.938	2.808	2.556
5	R2–Z (apex)	2.611	2.727	2.410
	Δ(4–5)	0.327	0.081	0.146
	av(4,5)	2.829	2.781	2.507

[a] Reference 7. [b] Reference 5.

to compete. Our results are also more host specific than seen before in that both yttrium and gadolinium appear to give only other condensed cluster phases.

Structure. The positional parameters for Pr_4I_5Ru are listed in Table III, while additional data appear as supplementary material. Other examples of this structure that were identified via indexing and lattice constant refinement of their unique powder patterns are given in Table I. The cell contents, atom numbering scheme, and the interchain bridging are shown in Figure 1, while a portion of one quasiinfinite chain is depicted in Figure 2. Important distances and angles are given in Table IV.

The structure type per se has been described in more detail for Y_4I_5C,[5] the heavy-atom positions for which are close to those originally described for (the presumably centered) Er_4I_5.[14] The chain (Figure 2) can be constructed by condensation of $Pr_6I_{12}Ru$ clusters through elimination of two trans, edge-bridging iodines and sharing of the remaining faces, namely one metal edge and the four inner iodine atoms on each of the side faces, to produce $^1_\infty[Pr_2Pr_{4/2}(Ru)I_{8/2}I_2]$. Additional and evidently essential bonding of iodine of all metal vertices also serves to interconnect the individual chains in two ways, Figure 1. All apex (Pr2) atoms are bonded to relatively distant $I2^{i-a}$ atoms in adjoining chains (displaced by $b/2$) in a mutually complementary manner so as to generate sheets of parallel chains in (001) with the apex Pr2 (and Ru) atoms lying approximately in the planes. These sheets are joined side by side by more tightly bound and approximately square-planar, shared $I3^{i-i}$ atoms that bridge side (Pr1–Pr1) edges of the nominal octahedra in parallel chains. (These iodines are not shown in Figure 2.)

The substitution of the large 4d element Ru in the R_4I_5Z chains has some interesting and unusual effects on the size and proportions of the nominal R octahedra and on the R–Z distances therein. For comparison, certain dimensional data for Pr_4I_5Ru are collected with those for Gd_4I_5Si and Y_4I_5C in Table V. It would be better if all of these were for the same R host, but Gd and Y did not form the ruthenide phase and the data for Gd_4I_5C have not been published.[7] However, the size differences over the

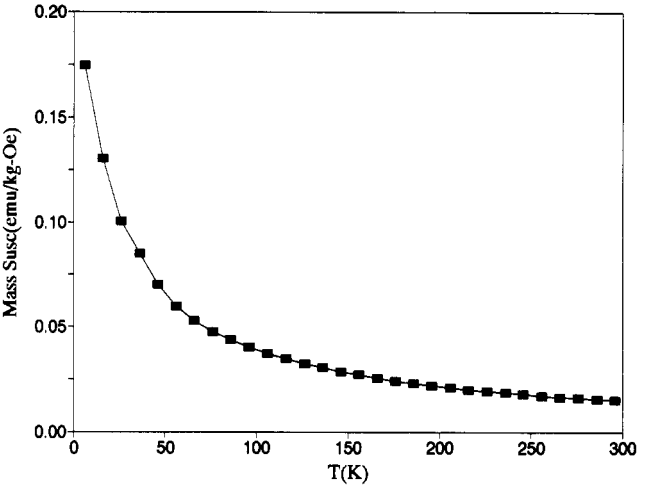

Figure 3. Mass susceptibility (emu/(kg Oe)) of Pr_4I_5Ru as a function of temperature.

series (Pr > Gd ≳ Y) parallel those of the corresponding Z and are fairly small, 0.028 Å in metallic[15] or about 0.10 Å in crystal radii overall.[16]

A major expansion of the clusters naturally accompanies the change in interstitials from Y_4I_5C to Pr_4I_5Ru; 0.32 Å in the average R–Z separation when the metallic radii are used to allow for the small change in host elements. As will be seen, silicon plays the role of a large main-group interstitial, almost as large as Ru. Because of this, the I···I distances within the iodine sheath on the chains are uniformly more "comfortable" closed-shell contacts with the larger Z, ≥4.20 Å vs 3.95 Å in the carbide. The interstitial change, particularly the variations in R2–Z at the apex, also appears to be the source of unusual variations in the interchain R2–$I2^{a-i}$ distances (Si, 3.146 Å; Ru, 3.450 Å; C, 3.503 Å). These decrease as the R2 apices protrude further above the surrounding iodides and permit shorter interchain bonding. The effect also appears as irregular relative increases in the *a* axis (Table I).

Some significant changes are found in the proportions within the clusters on variation of the interstitial. The most remarkable is in the relative length and presumably the strength of the apical R2–Z. That with ruthenium is 0.33 Å *less* than that to the waist (Pr1) atoms, vs a 0.15 Å difference in the carbide, and only 0.08 Å in Gd_4I_4Si. In other terms, the conversion of Gd_4I_5Si to Pr_4I_5Ru results in an increase of R1–Z by 0.13 Å while the apical R2–Z decreases by nearly 0.12 Å. The small difference in radii of Gd and Pr does not alter the contrast. A positive value for d(R1–Z) − d(R2–Z) in each octahedral unit is reasonable in the sense that the apex (R2) atoms have more iodine neighbors (five vs four) and fewer metal neighbors (four vs five) than those about the waist. However, the magnitude of the difference with Ru and its contrast with the main-group example is noteworthy; we conclude (below) that the reason is electronic.

Octahedral proportions reflecting more than changes in the bonding about Z are also seen. What was formerly the short shared edge of the octahedra (R1–R1) relative to the waist–apex (R1–R2) separation, by 0.26 Å in Y_4I_5C and 0.18 Å in Gd_4I_5Si, is now 0.11 Å *greater*. The relative elongation of the octahedra along the chain repeat also decreases with the larger Z. The greater chain repeat and short shared edge for small Z are natural consequences of not just probable closed-shell anion contacts along the chain but, particularly, of both d orbital symmetry and the larger number of metal neighbors above the R1 atoms in the shared edges.[17]

The d(Pr–Ru) found in Pr_4I_5Ru, 2.83 Å, is comparable to those calculated as before[2] for trigonal-prismatic environments about Ru in intermetallics, Pr_5Ru_2 (2.81 Å), and Pr_3Ru (2.94 Å).[18] This

(14) Berroth, K.; Simon, A. *J. Less-Common Met.* **1980**, *76*, 41.
(15) Corbett, J. D. *J. Solid State Chem.* **1981**, *37*, 337.
(16) Shannon, R. D. *Acta Crystallogr.* **1976**, *A32*, 751.
(17) Hughbanks, T.; Hoffmann, R. *J. Am. Chem. Soc.* **1983**, *105*, 3528.
(18) Palenzona, A. *J. Less-Common Met.* **1979**, *66*, P27.

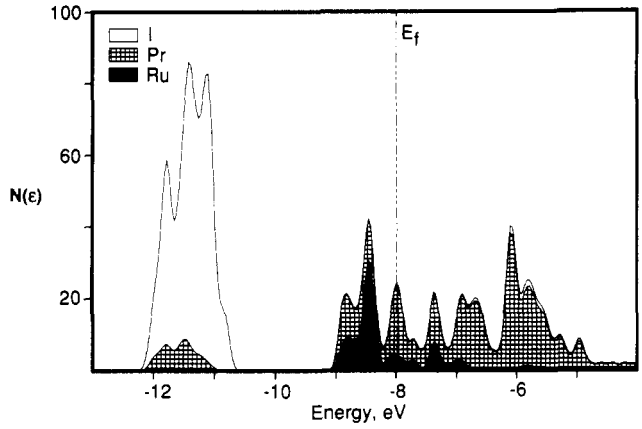

Figure 4. Densities-of-states diagram for Pr_4I_5Ru with atomic contributions by Ru (solid), Pr (hatched), and I (open) projected out.

is in distinct contrast to the differences commonly seen in the more oxidized cluster phases where host–Z distances are upward of 0.2 Å *less* than in comparable intermetallics,[1-3] e.g., 2.69 Å in $Y_6I_{10}Ru$ vs 2.85 and 2.86 Å in the yttrium–ruthenium compounds analogous to those above. An enhanced screening in the chains as in the binary ruthenium phases still seems qualitatively reasonable.

Magnetic Data. The magnetic susceptibility data for Pr_4I_5Ru are shown in Figure 3. The paramagnetic property illustrated follows the Curie–Weiss law over the entire temperature range with a Weiss constant θ of −20.8 K. The data yield a magnetic moment of 7.1 μ_B for Pr_4I_5Ru, or 1.8 μ_B/Pr atom. The result is an interesting contrast to the classical moment of the Pr^{3+} ion ($4f^2$, $^3H_4$), 3.58 μ_B.[19] A novel coupling of the $4f^2$ core moments of Pr, presumably via the delocalized Pr 5d + Ru 4d bonding system, is clearly present. We have not considered this in any further detail. The lanthanum analogue La_4I_5Ru displays a very small and virtually temperature-independent diamagnetism, $\sim 1.4 \times 10^{-4}$ emu/(mol Oe), which yields $\sim 5.0 \times 10^{-4}$ emu/(mol Oe) with core corrections. The lanthanum result is consistent with Pauli paramagnetism and the metallic character predicted by band calculations (below).

Bonding. The four relatively large Pr(waist)–Pr(apex) distances around each praseodymium in Pr_4I_5Ru suggest fairly weak Pr–Pr bonding, corresponding to an average Pauling bond order of only 0.087. Thus, one gains the distinct impression that the process of changing the interstitial from C to Ru results in a substantial loss of R–R bonding within the host cluster. The presumption is that this loss is replaced by stronger R–Z bonding, although in fact the competing alternative phases that actually determine stability are apt to be very different too. An equally profound change in the electronic structures appears to accompany the change in Z. Carbon 2p valence orbitals contribute only to the low-lying valence band in Y_4I_5C, reflecting strong Y–C bonding, whereas the conduction band contains virtually only Y–Y interactions.[5] In contrast, the higher lying ruthenium d orbitals may provide significant contributions to the conduction band in Pr_4I_5Ru, an attractive feature to us in that these states can presumably be altered to some degree by the choice of interstitial. These aspects have prompted us to examine the bonding in Pr_4I_5Ru as described by extended-Hückel band methods.

Figures 4 and 5 show the DOS (densities-of-states) and COOP (crystal orbital overlap population) curves for the model chain $^1_\infty[Pr_4I_8Ru^{3-}]$. Individual contributions for Pr (5d, 6s, 6p), I (5p), and Ru (4d, 5s) are projected out in the former; I 5s is off scale at lower energies, while Ru 5p contributions are very small up to E_F. Figure 5 highlights particular overlap-weighted pair populations: (A) Pr(eq)–I and Pr(ap)–I, (B) Pr(eq)–Ru and Pr(ap)–Ru, and (C) Pr(eq)–Pr(eq) (the shared edge) and Pr(eq)–Pr(ap) [(Pr(eq) = Pr1, Pr(ap) = Pr2)]. The large peak in the DOS curve between −12.5 and −10.5 eV consists mainly of

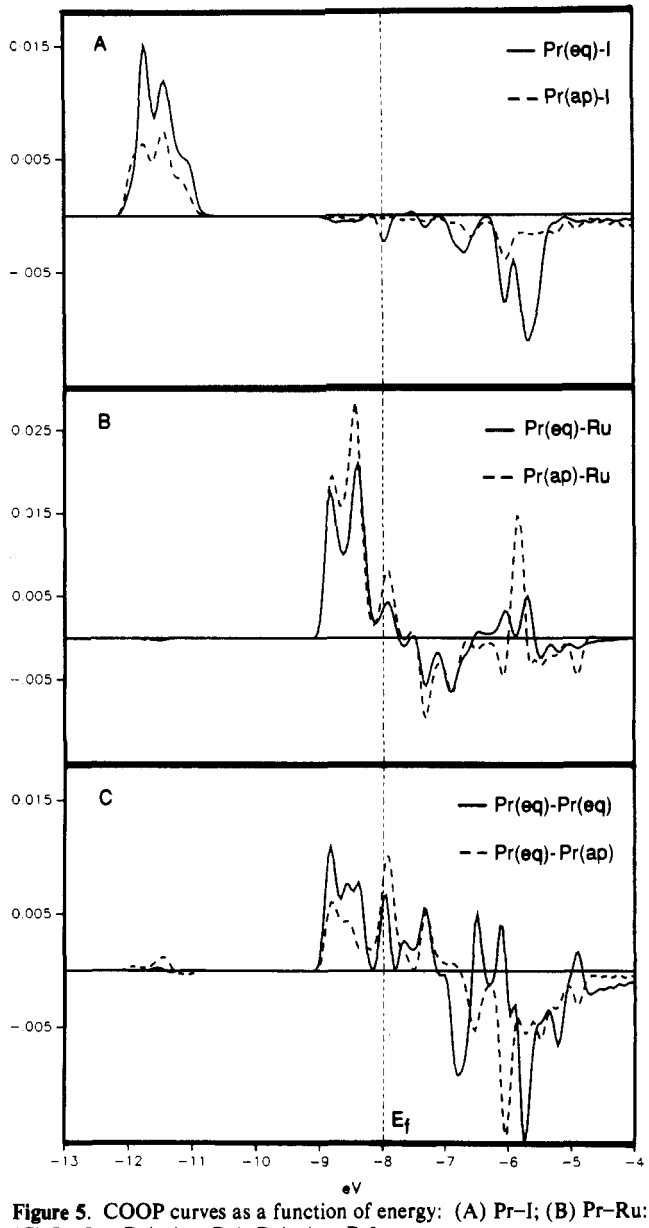

Figure 5. COOP curves as a function of energy: (A) Pr–I; (B) Pr–Ru: (C) Pr–Pr. Pr(eq) = Pr1, Pr(ap) = Pr2.

iodine p oribtals but includes appreciable praseodymium 5d as well, the strong Pr–I overlap reflecting the covalent bonding associated with iodine sheathing of the metal chain (Figure 5A).

The Fermi level at −7.98 eV crosses a region of high density of states. The large band just below (−8.25 to −9.25 eV) contains substantial Pr–Ru interactions—naturally greater for the shorter Pr2–Ru than for Pr1–Ru—together with concomitant equatorial Pr1–Pr1 and lesser Pr1–Pr2 bonding. These bands originate, in part, from strong Pr1 d_{xy}–Ru d_{xy}, Pr2 d_{z^2}–Ru d_{z^2}, and Pr2 d_{xz}, d_{yz}–Ru d_{xz}, d_{yz} orbital overlaps flavored with Pr1–Pr1 and, to a lesser extent, Pr1–Pr2 contributions. The effects are clearly summarized in Figure 5B (Pr–Ru) and Figure 5C (Pr–Pr). Each COOP function represents a single atom pair interaction, so the relative contributions of Pr1–Ru and Pr1–Pr2 should be multiplied by frequency factors of 2 and 4 to judge their importances relative to Pr2–Ru and Pr1–Pr1, respectively. (The two types cannot be intercompared, however, because of the necessarily different overlap integrals.)

An enlarged portion of the DOS curve near the Fermi level is shown in Figure 6 together with the corresponding portion of the band diagram to illustrate how the bands run from Γ to *X*. The bands are given two-letter labels according to their symmetry with respect to the *xz* and *xy* planes in the ideal model (S = symmetric, A = antisymmetric). (The crossing of the bands marked AS and SA near E_F is avoided in the real structure.) The oribtal con-

(19) Kittel, C. *Introduction to Solid State Physics*, 6th ed.; J. Wiley: New York, 1986; p 405.

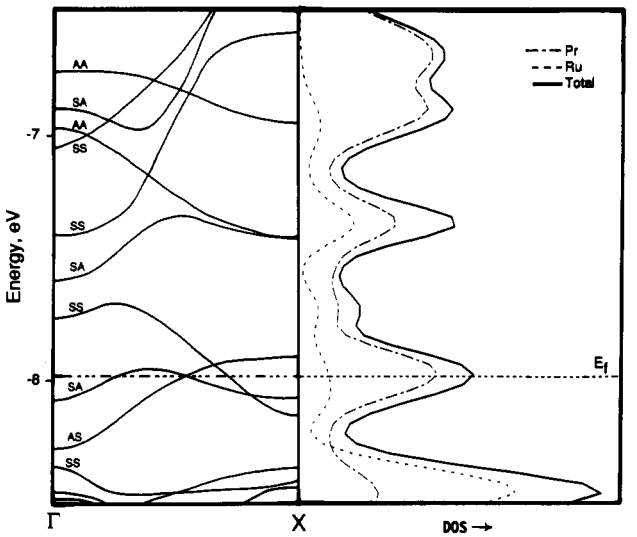

Figure 6. Left: energy bands along the chain and near E_F in Pr_4I_5Ru. Right: DOS in the same region with Ru (---) and Pr (— — —) contributions.

tributions to the three bands crossing the Fermi level are shown in I together with their corresponding symmetries. These three

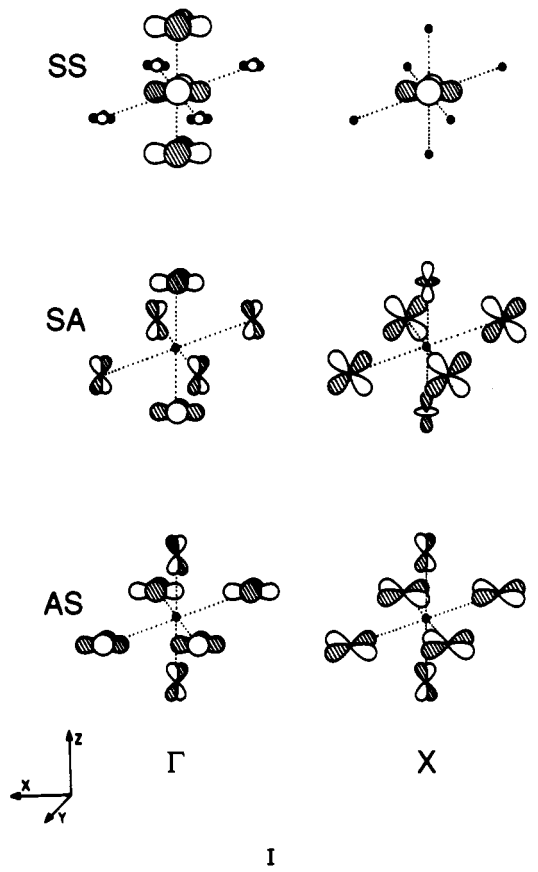

I

bands exhibit mainly Pr–Pr bonding, nonbonding, and antibonding effects. Only one band has Ru character, nonbonding in the occupied portion and δ^* bonding above. At the present time the choice of Z in this host and structure is limited to Co, Ru, and Os, and it is only within this group that the nature of the states at E_F could be altered.

The energy bands in this region (Figure 6, left) actually exhibit a small (0.2 eV) gap between the above Pr–Ru states and the conduction band states nearer E_F, and so the former feature probably ought to be termed an upper or metal valence band. The gap is not required by symmetry, even for the real structure, and its presence or not is presumably sensitive to parameters used for Pr and Ru, so the result probably should not be taken too seriously.

The charges that develop on the atoms in this calculation are indicative of the covalent nature of the bonding, although their quantitative values should not be taken too literally. Both Pr and the interstitial Ru have calculated positive charges of ~+0.2 to +0.4 in the Mulliken bond/atom population sense. The charge similarity for interstitial Ru relative to Pr seems reasonable in the sense that some of the Ru d orbitals appear less completely bonded (below). The finer details of these charge distribution approximations are naturally sensitive to the H_{ii} values used and, to a lesser extent, the orbital parameters and thence overlap integrals. We found that the use of distinctly higher H_{ii} values for Pr based on $LaCp_2$ (−6.43 eV for Pr 3d)[12] together with a self-consistent value for Ru from $Y_6I_{10}Ru$[3] resulted in unreasonable polarity and a charge of −1.4 on Ru. The iteration performed was to reflect the real variation of H_{ii} (5d mainly) with population based on spectroscopic data for the gaseous element. An even more extreme charge (−3) was found earlier for iron in a $Zr_6I_{18}Fe^{4-}$ cluster calculation when conventional H_{ii} data for cationic iron were utilized without iteration.[20]

Our results differ in a reasonable way from those reported for the isostructural Gd_4I_4Si.[7] Here a narrow Si (+Gd) valence band was calculated to be centered about 2 eV below the bottom of the conduction band and about 1 eV above the top of the I (+Gd) valence band. Calculated atom charges and the self consistency of the model were not noted. Our EHMO calculations on an isolated $Zr_6I_{18}Si^{4-}$ cluster (utilizing the same Si parameters) placed the Si (+Zr) t_{1u} band at the top of the iodine valence band,[21] a reasonable comparison. Differences in the qualitative *interpretation* of the bonding in Gd_4I_5Si are more substantial. The silicide was described in terms of a very heteropolar model with strong ionic interactions, including repulsion between formal Si^{4-} ions along the chain. Although the last describes the oxidation state of silicon well (since all 3p orbitals are filled), it must be far from actuality in terms of charge distributions. The oxidation state–charge contrasts have been well considered by Sleight[22] in another context.

Finally, a markedly different mode of distortion of the condensed clusters is found in Pr_4I_5Ru relative to Gd_4I_5Si. The increased size of Z leads to a noticeable reduction in the largest inequality among the octahedral edges such that the shared edge relative to the axial repeat differ by only 0.22 Å vs 0.46 Å before (Table V). The average waist–apex distance scarcely changes in the process, and the result is much more uniform R–R distances and bonding about the octahedral edges, the average overlap population per R–R edge being rather low, ~0.13, or if you prefer, with a Pauling bond order of 0.066 per edge. On the other hand, the two Pr–Ru distances differ by 0.327 Å, corresponding to orbital populations of 0.28 for the longer (and twice as numerous) Pr1–Ru distances within the plane of the shared edges and of 0.41 for distances to the nearer apices (Pr2–Ru). This parallels the impression noted earlier than the bonding of the chain in this case appears to be much more Pr–Ru than Pr–Pr. (The importance of Pr–I must be acknowledged as well; these overlap populations within the chain (Figure 2) average ~0.36.)

Differences in bonding capabilities of the main-group Si vs transition element Ru must be responsible for the marked changes in the R–Z proportions, namely a 0.24-Å increase in Δd(R–Z) with Ru. Although dimensional disparities within the octahedra appear to be a "given" for this mode of cluster condensation,[17] the consequences of a switch from s and p bonding orbitals on silicon to d (and s) on ruthenium emphasizes this. Two orbitals on Ru (d_{z^2} and d_{xy} in our coordinate system) are especially effective for σ bonding. The remaining three, d_{xz}, d_{yz}, and $d_{x^2-y^2}$, provide less effective π (and σ) bonding to the Pr neighbors that is in degree distinctly dependent on the asymmetry of the octahedra. These effects are reflected in the lower populations calculated for these orbitals with the clear trend $d_{x^2-y^2} > d_{xz} > d_{yz}$. As shown

(20) Hughbanks, T.; Rosenthal, G.; Corbett, J. D. *J. Am. Chem. Soc.* **1988**, *110*, 1511.
(21) Smith, J. D.; Corbett, J. D. *J. Am. Chem. Soc.* **1986**, *108*, 1927.
(22) Sleight, A. W. *Proc. Welch Fndn. Conf. Chem. Res.* **1988**, *32*, 123.

in II, the elongation of the octahedra along the chain (dashed)

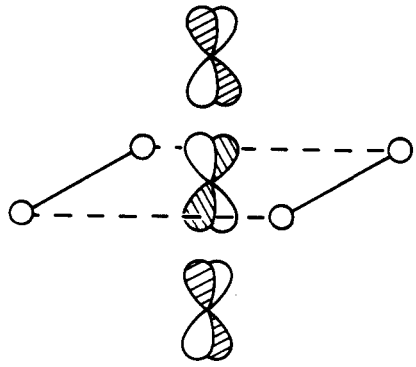

II

means that the d_{yz} orbital in particular is most effective in bonding axial Pr to Ru, thereby enhancing the observed Pr-Ru bonding distortion. These distinctions would not enter in with a main-group interstitial.

Recognition of the versatility of interstitially stabilized clusters and condensed clusters continues apace, and the complexity of the synthetic problems is increasing too. For example, just the components Pr, Os, and I are known to produce four ternary cluster and condensed cluster phases. The most important factor determining the stability, or not, of these compounds appears to be the stability of alternate phases. The absence of, for example, a Pr_4I_5Z phase for Z = Re, Ir, Rh, Pt, Fe, or Cu, all of which are known as $Pr_7I_{12}Z$, and of any cluster compound for Z = Ag is accordingly very difficult to explain or correlate. Obviously, theoretical calculations will not provide electronic "explanations" unless the stabilities of all alternatives can also be considered in a reliable way. Even trends with Z when no other cluster phases exist may be complex in origin when binary R-Z components change with the selection of interstitial.

Acknowledgment. Arnold Guloy provided considerable assistance in the calculational part of the research. Jerome Ostensen was instrumental in securing the magnetic susceptibility data. This research was supported by the National Science Foundation, Solid State Chemistry, via Grants DMR-8318616 and -8902954, and was carried out in facilities of Ames Laboratory, DOE.

Supplementary Material Available: Tables of data collection and refinement details and anisotropic thermal parameters for Pr_4I_5Ru (2 pages); a table of structure factor data for Pr_4I_5Ru (6 pages). Ordering information is given on any current masthead page.

Contribution from the Department of Chemistry,
Macalester College, St. Paul, Minnesota 55105

Crystal Structure of a Novel Copper(I) Cyanide Complex with Hexamethylenetetramine, $(CuCN)_3(C_6H_{12}N_4)_2$

Fred B. Stocker

Received July 23, 1990

The crystal structure of $(CuCN)_3(C_6H_{12}N_4)_2$ (**1**) consists of infinite chains of alternating copper(I) and CN which are bound into infinite sheets by hexamethylenetetramine. The CN groups appear to be totally end-for-end disordered. The preparation of the complex is unusual by the fact that none of the final constituent species is present in the starting material; i.e. the copper(I) ion, the cyanide ion, and the hexamethylenetetramine are all created in situ. The crystal is monoclinic, space group $C2/c$, with a = 14.812 (10) Å, b = 11.445 (3) Å, c = 14.784 (7) Å, β = 126.78 (5)°, and Z = 4; R was 0.042 for 2065 independent reflections.

Introduction

While performing an adaptation of the Parrod synthesis[1-4] of imidazoles (Scheme I), which normally employs hexoses (especially D-fructose) with copper(II) salts, ammonia, and formaldehyde, I inadvertently discovered a novel copper complex. In my adaptation I planned to hydrolyze sucrose to form a mixture of glucose/fructose prior to performing the Parrod synthesis (Scheme II). On one occasion during my preliminary work on this modification, sucrose was inadvertently used in the Parrod synthesis due to an error in the hydrolysis experiment. Instead of the expected olive brown precipitate of the sparingly soluble copper-imidazole complex, colorless needles began separating out of the deep blue aqueous solution shortly after the temperature reached 85-90 °C. The slow production of the crystalline product continued over the 8-h reaction period. That this material contained copper was shown by its dissolution in nitric acid to produce a blue solution that turned to deep blue in the presence of ammonia. Although I knew of no pathway consistent with current theory that would allow a nonreducing sugar such as sucrose to react in a Parrod synthesis, I repeated the reaction with sucrose (omitting the hydrolysis procedure) several times before definitive analytical data became available on the new complex. When

Scheme I

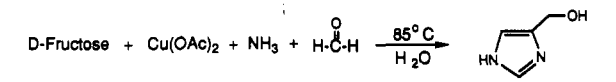

(Isolated as cuprous salt)

Scheme II

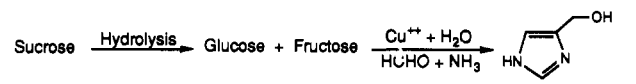

(Isolated as cuprous salt)

elemental analysis confirmed the presence of copper, carbon, hydrogen, and nitrogen and the absence of oxygen, I felt certain that sucrose was not involved in the reaction. I confirmed that theory by isolating the complex from a reaction system that omitted sucrose (Scheme III).

Scheme III

$$Cu(OAc)_2 + NH_3 + HCHO \xrightarrow[H_2O]{85\ ^\circ C} (CuCN)_3(C_6H_{12}N_4)_2$$

The physical properties of the salt were quite interesting. It was found to be very stable under atmospheric conditions and highly insoluble in all the common solvents including water, acetone, lower alcohols, DMSO, DMF, acetonitrile, haloalkanes, aromatics, etc. The infrared spectrum of the salt revealed a strong cyanide vibration (KBr 2075 cm^{-1}, Nujol 2070 cm^{-1}) and a magnetic susceptibility study showed the salt to be diamagnetic, consistent with its absence of color.

(1) Parrod, J. *Bull. Soc. Chim. Fr.* **1932**, *51*, 1424
(2) Horning, E. C. *Organic Syntheses*; John Wiley and Sons, Inc.: New York, 1944, Vol. 24, p 64.
(3) Weidenhagen, R.; Herrmann, R.; Wegner, H. *Ber. Dtsch. Chem. Ges. B* **1937**, *70*, 570.
(4) Hofmann, J. *Imidazole and Derivatives*; Interscience Inc.: New York, 1953; Part I, pp 102-106.

0020-1669/91/1330-1472$02.50/0